water

MDPI

Article

Hydrologic Assessment of TRMM and GPM-Based Precipitation Products in Transboundary River Catchment (Chenab River, Pakistan)

Ehtesham Ahmed [1,*], Firas Al Janabi [1], Jin Zhang [2], Wenyu Yang [3], Naeem Saddique [4] and Peter Krebs [1]

1 Institute of Urban and Industrial Water Management, Technische Universität Dresden, 01069 Dresden, Germany; firas.aljanabi@tu-dresden.de (F.A.J.); peter.krebs@tu-dresden.de (P.K.)
2 Institute of Groundwater and Earth Sciences, Jinan University, Guangzhou 510632, China; jzhang@jnu.edu.cn
3 Institute of Environmental Sciences, Brandenburgische Technische Universität, 03046 Cottbus, Germany; steineryang@163.com
4 Institute of Hydrology and Meteorology, Technische Universität Dresden, 01062 Dresden, Germany; naeem.saddique@tu-dresden.de
* Correspondence: ehtesham.ahmed@tu-dresden.de; Tel.: +49-1525-6918549

Received: 9 June 2020; Accepted: 1 July 2020; Published: 3 July 2020

Abstract: Water resources planning and management depend on the quality of climatic data, particularly rainfall data, for reliable hydrological modeling. This can be very problematic in transboundary rivers with limited disclosing of data among the riparian countries. Satellite precipitation products are recognized as a promising source to substitute the ground-based observations in these conditions. This research aims to assess the feasibility of using a satellite-based precipitation product for better hydrological modeling in an ungauged and riparian river in Pakistan, i.e., the Chenab River. A semidistributed hydrological model of The soil and water assessment tool (SWAT) was set up and two renowned satellite precipitation products, i.e., global precipitation mission (GPM) IMERG-F v6 and tropical rainfall measuring mission (TRMM) 3B42 v7, were selected to assess the runoff pattern in Chenab River. The calibration was done from 2001–2006 with two years of a warmup period. The validation (2007–2010) results exhibit higher correlation between observed and simulated discharges at monthly timescale simulations, IMERG-F (R^2 = 0.89, NSE = 0.82), 3B42 (R^2 = 0.85, NSE = 0.72), rather than daily timescale simulations, IMERG-F (R^2 = 0.66, NSE = 0.61), 3B42 (R^2 = 0.64, NSE = 0.54). Moreover, the comparison between IMERG-F and 3B42, shows that IMERG-F is superior to 3B42 by indicating higher R^2, NSE and lower percent bias (PBIAS) at both monthly and daily timescale. The results are strengthened by Taylor diagram statistics, which represent a higher correlation (R) and less RMS error between observed and simulated values for IMERG-F. IMERG-F has great potential utility in the Chenab River catchment as it outperformed the 3B42 precipitation in this study. However, its poor skill of capturing peaks at daily timescale remains, leaving a room for IMERG-F to improve its algorithm in the upcoming release.

Keywords: TRMM 3B42 v7; GPM IMERG-F v6; Chenab River; satellite precipitation; ungauged catchment; transboundary river

1. Introduction

Satellite Precipitation has gone through two renowned satellite products, named as, tropical rainfall measuring mission (TRMM) [1] and global precipitation measurement (GPM) [2]. These products were estimated using TRMM multi-satellite precipitation analysis (TMPA) [1] and integrated multi-satellite retrievals for GPM (IMERG) [2], respectively. IMERG is available in finer spatial (0.1° × 0.1°) resolution than TMPA spatial (0.25° × 0.25°) resolution. This study emphasizes the use of these two satellite

products on an ungauged catchment of the Chenab River in Pakistan. There are a large number of studies [3–10] have been done in sparsely or ungauged catchments using satellite-based products to estimate the river or stream discharges. This study focuses on the catchment of the Chenab River that is completely ungauged. Five major rivers flow through Pakistan: Indus, Jhelum, Chenab, Ravi and Sutlej. These rivers come from transboundary Indian catchments [11,12]. Indus is the biggest river, which is fed by the Chenab River as a major tributary (Figure 1). River Chenab is a transboundary and ungauged river whose flood and gauge precipitation information is not easy to collect from the Indian side. Owing to the active Monsoon belt of Pir Punjal [13], the Chenab River catchment suffers from severe floods almost every year since the last decade [14], causing massive damage to local society. The recent advances in satellite-based precipitation retrieving missions have overcome the problems of water managers to attain alternative precipitation information for flood simulations in ungauged basins. In comparison to the GPM era, TRMM precipitation was used widely in hydrological modeling in most parts of the world [15–22]. TMPA is a reliable and most extensively used satellite product in the TRMM era [23,24]. Several studies show that TMPA has satisfactory or acceptable results in many parts of the world [15–22].

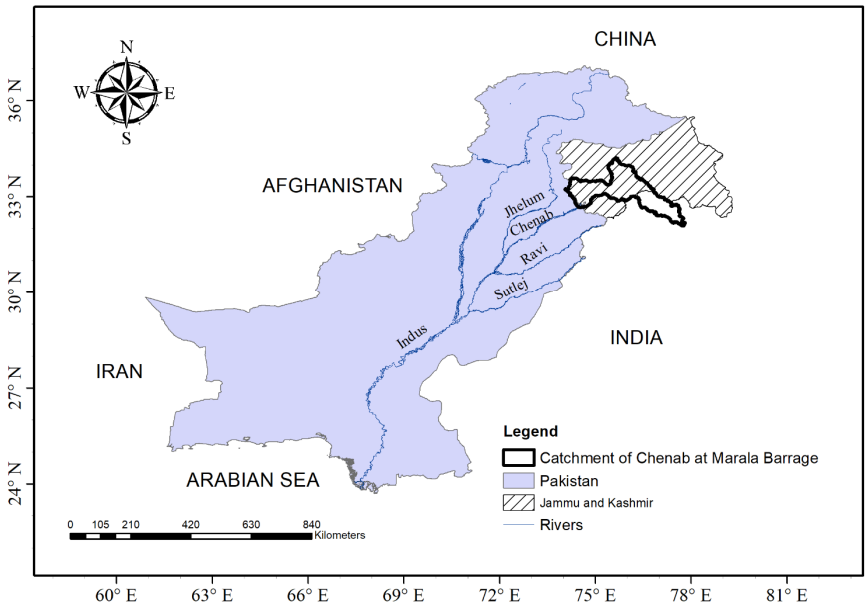

Figure 1. Location map of the Indus basin rivers and the Chenab catchment.

The GPM mission, the successor to the TRMM era, was officially launched by The National Aeronautics and Space Administration (NASA) and the Japan Aerospace Exploration Agency (JAXA) in February 2014 and hence, TRMM mission ended in April 2015. NASA released IMERG, its first GPM era precipitation product, in March 2014. IMERG provides more expansive quasi-global (60° N–60° S) and spatiotemporal (0.1° × 0.1° and 30 min interval) coverage than TMPA [25]. It includes three products: the near real-time "Early" run (IMERG-E), "Late" run (IMERG-L) and "Final" run (IMERG-F) [25]. Many previous researchers concluded that GPM-IMERG has batter accuracy than TRMM-TMPA [26–30].

Anjum et al. [31] compared the TMPA products, i.e., 3B42 v7 and 3B42RT with IMERG and indicated that IMERG precipitation is more reliable than TMPA estimates. Moreover, IMERG estimates capture the spatial distribution of precipitation more realistically than TMPA estimates over the highlands of northern areas of Pakistan. Rozante et al. [32] highlighted that IMERG products are a batter replacement of TMPA products in several regions containing different precipitation patterns in Brazil. Prakash et al. [26] studied the utility of IMERG and TMPA products in India during the Monsoon season (June 2014–September 2014). Their study showed that IMERG estimates represent a more realistic variability than gauge adjusted TMPA estimates. Tan et al. [33] demonstrated that IMERG near-real-time products, consisting of finer spatial and temporal resolution than TMPA products,

can be regarded as reliable satellite precipitation products to study the 2014–2015 flood event in Malaysia. Prakash et al. [34] investigated heavy rainfall over India in which TMPA overestimated the heavy rainfall events (above 75th percent of observed data), whereas IMERG shows remarkable improvements for Southwest Monsoon season. In Tehran and Kermanshah, with orographic and stratiform precipitation pattern, IMERG yields sound results for precipitation detection on the basis of probability of detection, critical success index and false alarm ratio [35]. Owing to enhanced precipitation techniques, several studies [36–38] indicated that IMERG estimates show better results than TRMM estimates.

This study focuses on the application of a GIS-based tool, The soil and water assessment tool (SWAT) [39,40]. It is a physical-based semidistributed hydrological model, which has been widely applied for river catchment discharge estimation around the world [41–44]. The selection of the best hydrologic model for discharge estimation is based on study objectives, characteristics of catchment, availability of data, required accuracy and ease in calibration [45]. SWAT model has several capabilities such as hydrologic process, soil erosion, pollutant transport, assessment of climate change effects, water management practices and land use change behavior [46–49]. Another computer program, SWAT calibration and uncertainty procedures (CUP), is used to calibrate the SWAT model [50]. The calibration process involves accessing the accuracy of hydrologic model simulation through sensitivity and uncertainty analysis [51]. Various techniques of uncertainties are explained by Yang et al. [52] for a better calibration process in Chaohe basin China. Yang et al. [52] compared the four algorithms: sequential uncertainty fitting (SUFI-2) [53,54], generalized likelihood uncertainty estimation (GLUE) [55], Parameter solutions (ParaSol) [56] and Markov chain Monte Carlo (MCMC) [57]. SWAT-CUP links these algorithms to the SWAT model and enables us to perform uncertainty analysis of model parameters. Rostamian et al. [58] performed uncertainty analysis using the SUFI2 algorithm for model runoff calibration in two mountainous basins in Iran. Setegn et al. [59] used GLUE, SUFI-2 and ParaSol in Lake Tana Basin to access the performance of the SWAT model. Yang et al. [52] applied the SUFI-2 algorithm in their study and concluded that SUFI-2 needs a less number of model simulations to attain good quality uncertainty analysis. The selection of the SWAT model, for this study, was also based on its ease and good quality calibration with SWAT-CUP by using the SUFI-2 algorithm.

From the viewpoint of the transboundary river, this study is useful as 97% of the catchment of the Chenab River, at Marala Barrage, i.e., the first rim station of the river entering Pakistan, lies in India and only 3% lies in Pakistan as shown in Figure 1. Due to present conflicts between India and Pakistan, in situ hydrometeorological data sharing is very limited between these two countries [60]. The overall goal of this study is hence to better understand the hydrological phenomenon of the riparian river, like the Chenab River in Pakistan, by using the open-source satellite-based hydrometeorological products, such as GPM IMERG-F and TRMM 3B42.

2. Study Area

River Chenab is fed by two main streams, i.e., the Bhaga and the Chandra in Himachal Pradesh in India and flows through Indian-controlled Jammu and Kashmir to enter Pakistan [61]. It has the first gauging site at Marala Barrage (74.46° E, 32.67° N) near Sialkot, Pakistan (Figure 2). The extent of the Chenab River catchment lies in 73°–78° E and 32°–35° N. The catchment of Chenab River covers an area of about 26,000 km^2 up to Marala Barrage (Figure 2). The elevation range of the catchment varies from 235 m near Marala Barrage to 7103 m in the upper snowy area [60]. Chenab River slope varies from 25 m/km in the uppermost part of the river to 0.4 m/km in the plains [62]. Singh et al. [63] divided the Chenab River catchment based on altitude and studied the spatial and seasonal variation in precipitation. They described that about 75% of rainfall occurs in the Greater Himalaya ranges during monsoon and pre-monsoon season, while 15% of rainfall occurs in the form of snowfall during winter. About 65% of rainfall occurs in Middle Himalaya ranges during monsoon and pre-monsoon season and about 26% of rainfall during the winter season. In Outer Himalaya ranges, about 36% of rainfall occurs during winter season in the form of seasonal rain instead of snow due to lower altitudes.

The major contribution of river flow in the mid or late summer season is from snowmelt, which is later enhanced by seasonal Monsoon rainfall. Due to this combined flow from snowmelt and precipitation, most of the peak flows occur in June–September [64]. Thus, there is a need to closely examine the hydrological pattern of discharges in Chenab River.

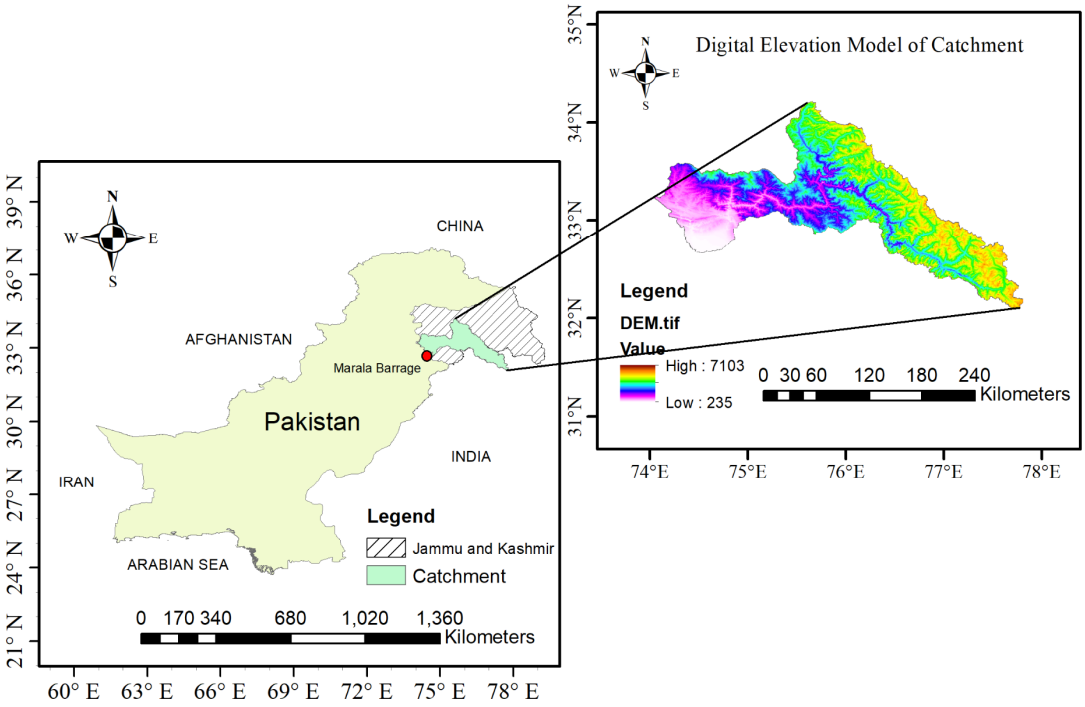

Figure 2. Visualization of the study area.

3. Data Description and Processing

3.1. Digital Elevation Data

The topography of the catchment is represented by a digital elevation model (DEM), which is used to delineate the catchment [65] and to analyze the flow path/drainage pattern of the land surfaces. Analysis of DEM helps to obtain the sub-catchments and stream or river parameters. In the present study, shuttle radar topography mission (SRTM) DEM with a 30 m spatial resolution was extracted from the weblink of Jet Propulsion Laboratory of National Aeronautics and Space Administration (NASA) https://www2.jpl.nasa.gov/srtm/.

3.2. Hydro-Climatic Data

NASA precipitation measuring missions, GPM and TRMM datasets, were downloaded from NASA earth data platform, i.e., GES DISC website: https://disc.gsfc.nasa.gov/. In this study, GPM-based IMERG final precipitation (version 6) (NASA Goddard Space Flight Center, Greenbelt, MD, USA) and TRMM-based TMPA-3B42 (version 7) (NASA Goddard Space Flight Center, Greenbelt, MD, USA) were downloaded from 2001–2010. Daily timescale datasets were downloaded and extracted for the Chenab River catchment for both IMERG-F and 3B42 precipitation products. Downloaded NetCDF (NC4) files were processed in ArcMap to get the average cumulative precipitation values for each sub-catchment at every timestep. A routine in ArcMap was developed, and the process automated to receive the precipitation values for each sub-catchment, as shown in Figure 3.

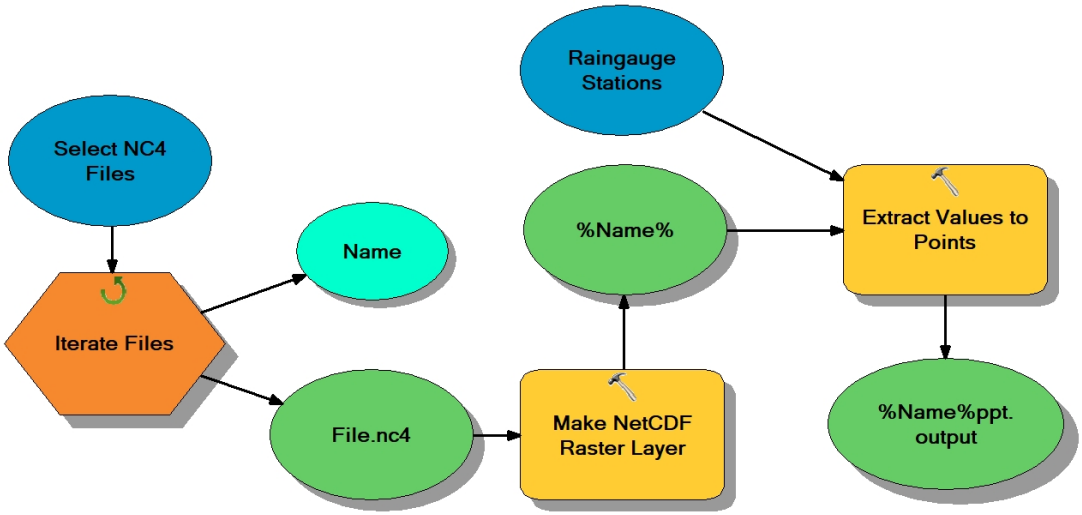

Figure 3. Satellite precipitation (NC4) files processing in ArcMap.

This procedure began with the "iterate files" tool by selecting repeated NC4 files according to the file names. Then, NC4 files were converted into raster layers, which were eventually processed in the "extract values to points" tool to extract the precipitation values according to a given rain gauge station shapefile. Rain gauge station shapefile was the centroid of each sub-catchment.

Maximum and minimum temperatures, relative humidity, sunshine duration and wind speed data were obtained from the climate forecast system reanalysis (CFSR) dataset. The CFSR dataset is developed by the National Centers for Environmental Prediction (NCEP) of The National Oceanic and Atmospheric Administration (NOAA) and can be retrieved from the weblink: https://www.ncdc.noaa.gov/. The CFSR is a fully coupled land-ocean–atmosphere model that uses numeric weather prediction techniques to assimilate atmospheric states [66]. Additionally, CFSR product has more horizontal resolution than any other reanalysis product [67].

Daily and monthly observed discharge at the Marala Barrage gauging site was required to compare the modeled and observed values. These data were obtained from the flood forecasting division of Pakistan Meteorological Department (PMD) and utilized for daily and monthly model calibration.

3.3. Land Use and Soil Type Data

Land use dataset are used to recognize the hydrological processes and their governing systems [68]. Digital identification of the study area (Figure 4) was done by dataset acquired from https://swat.tamu.edu/data/. Seventeen different types of land use classes are present in the study area catchment, which are shown in Table 1. The major part of land use was grassland (20.55%) followed by shrubland (15.71%), irrigated croplands and pasture (15.24%) and snow or ice (12.18%), as displayed in Figure 4.

Another important aspect of recognizing the hydrologic responses is soil type and texture [69]. Soil type data (Figure 5) was downloaded from the United Nations Food and Agriculture Organization (FAO) harmonized world soil database (HWSD), http://www.fao.org/home/en/. The HWSD consists of 30 resolution with more than 15,000 different soil-mapping units. The soil type classification of the study area is presented in Table 2, describing eight different types of soils. Chenab catchment consists of 40.87% of lithic soils followed by orthic luvisol (20.03%), glaciers (18.3%) and haplic phaeozem (12.51%). lithic soils are present in the middle range of the catchment, while glaciers and haplic phaeozem cover the upper range of the catchment Figure 5.

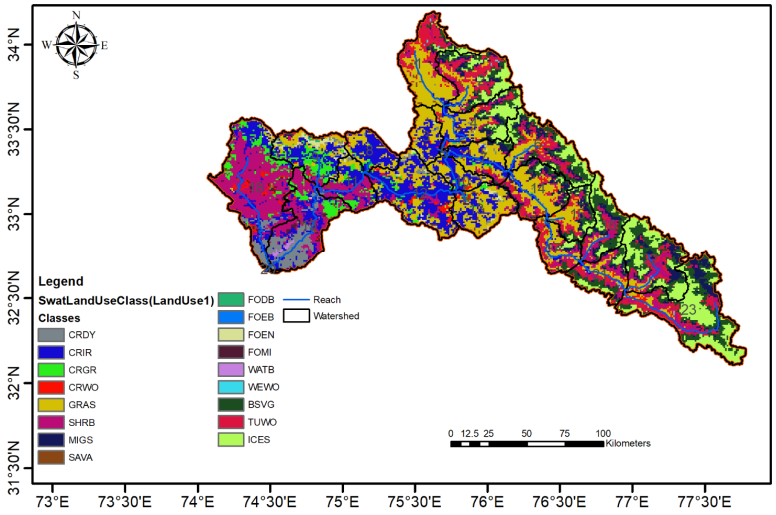

Figure 4. Land use map of the study area.

Table 1. Land use classification in the study area.

Land Use Class	Class Description	Area (km^2)	% Area
GRAS	Grassland	5389.3	20.55
SHRB	Shrubland	4119.72	15.71
CRIR	Irrigated cropland and pasture	3995.3	15.24
ICES	Snow or ice	3193.61	12.18
BSVG	Barren or sparsely vegetated	2698.42	10.29
TUWO	Wooded tundra	2099.03	8
MIGS	Mixed grassland/shrubland	1516.36	5.78
CRGR	Cropland/grassland mosaic	1070.04	4.08
CRDY	Dryland cropland and pasture	1041.24	3.97
CRWO	Cropland/woodland mosaic	441.65	1.68
FEN	Evergreen needleleaf forest	247.9	0.95
SAVA	Savanna	164.11	0.63
FOMI	Mixed forest	131.91	0.5
FODB	Deciduous broadleaf forest	50.51	0.19
WATB	Water bodies	39.24	0.15
WEWO	Wooded wetland	22.61	0.09
FEB	Evergreen broadleaf forest	2.95	0.01

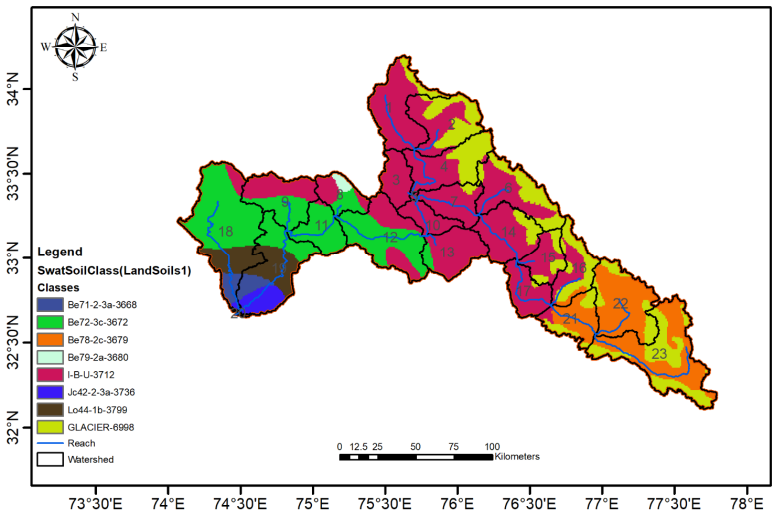

Figure 5. Soil type map of the study area.

Table 2. Soil classification in the study area.

Soil Class	Soil Texture	Associated Soil	Area (km^2)	% Area
I-B-U-3712	Loam	Lithic	10,718.13	40.87
Be72-3c-3672	Clay	Orthic luvisol	5253.41	20.03
GLACIER-6998	UWB	glacier	4799.72	18.3
Be78-2c-3679	Loam	Haplic phaeozem	3279.61	12.51
Lo44-1b-3799	Sandy Loam	Chromic luvisol	1188.51	4.53
Jc42-2/3a-3736	Clay Loam	Eutric fluvisols	461.04	1.76
Be71-2-3a-3668	Clay Loam	Gleyic cambisol	418.43	1.6
Be79-2a-3680	Loam	Eutric gleysol	105.8	0.4

4. Methods

In this study, the methodology was devised based on open-source datasets in an ungauged Chenab River catchment. Thus, the hydrological model developed is based on different open-source datasets for topography, soil, land use and precipitation, as described in the previous section.

4.1. Hydrologic Simulation Using SWAT Model

Flow modeling in ungauged and large catchments is a very challenging task for water managers in developing countries [70]. The soil and water assessment tool (SWAT) was designed by the US Department of Agriculture—agricultural research services (USDA-ARS) to manage the water resources from large river basins [40]. SWAT model has also been widely used in the hydrological modeling of ungauged basins [5,6,71]. It is a physical-based, time-continuous and semidistributed hydrologic model [72]. In the SWAT model, the whole catchment is divided into sub-catchments, which are then further subdivided into hydrological response units (HRUs). The HRUs are the basic elements of hydrological estimations, which integrate land use, soil type and topography. The hydrological processes within SWAT consist of infiltration, lateral flow, plant uptake, evaporation and snowmelt [73]. These processes are simulated in SWAT-based on the water balance equation. The soil conservation services (SCS) curve number method was used to calculate the surface discharge. The channel flow rate and velocity are obtained by using Manning's equation, whereas lateral flow is estimated by the kinematic storage model. The Hargreaves method was employed for the estimation of evapotranspiration. Further details can be from the SWAT user manual [73].

SWAT requires spatial data, such as DEM, land use, soil type and slope classification. All of these datasets were projected to a similar coordinate system in ArcMap. The Arc-SWAT 2012 was used to simulate the hydrologic process in the Chenab River catchment using open source data spatial and climatic data. The DEM was used to delineate the catchment into 23 sub-catchments (Figure 6), while spatial datasets, e.g., land use, soil type and slope were used to generate 1792 lumped areas or HRUs.

To consider the snowmelt effect in SWAT, five elevation bands were introduced in sub-catchments. Two open-source climatic datasets, i.e., IMERG-F v6 and 3B42 v7, were used in the model to simulate the flow in the catchment at daily and monthly timescale. SWAT model was calibrated from 2003–2006 and validated from 2007–2010. A two-year (2001–2002) warmup period was applied to stabilize the model.

4.2. Sensitivity/Uncertainty Analysis

SWAT-CUP was developed by Abbaspour [50] to ease the uncertainty/sensitivity analysis, calibration and validation processes. In this study, the SUFI-2 algorithm was used to perform sensitivity and uncertainty analysis in simulated flows of the SWAT model. A widely used autocalibration algorithm, SUFI-2, provides comparable results for sensitivity analysis, calibration, validation [52]. Yang et al. [52] described the procedure to calculate the parameter sensitivities by using a multiple regression system with Latin hypercube sampling utilizing objective function values.

Several objective functions have been used so far to estimate the model performance, for example, the R^2, the Nash–Sutcliffe efficiency (NSE), the chi-squared and root mean square error. In this study, NSE was chosen as an objective function and global sensitivity analysis (GSA) was performed to check the sensitivity of an individual parameter.

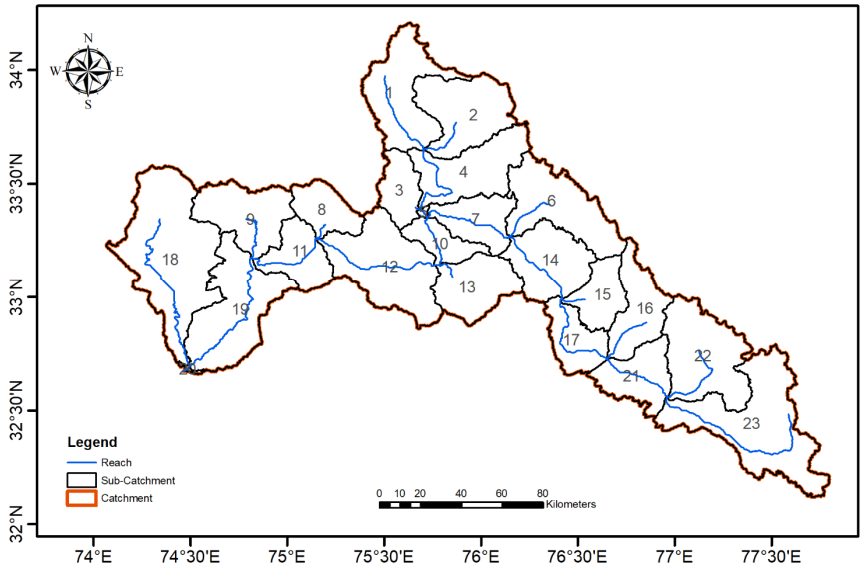

Figure 6. Delineation of the study catchment.

Global Sensitivity Analysis (GSA)

A global sensitivity analysis (GSA) was performed for the control point, i.e., the Marala Barrage gauging site of the study area, to find the most responsive model parameters. For GSA, seventeen parameters were selected and 1000 simulations were run. The SUFI-2 algorithm was applied to categorize the most active ten parameters from a list of seventeen parameters. A *t*-test was applied to identify the relative significance of the parameters. The *t*-stat and P-value enable us to elect the parameter according to its sensitivity. The larger the value of *t*-stat and lower the value of P make the parameter more sensitive (Figure 7). Parameters, CH_K2, CH_N2, followed by CN2 and ALPHA_BF were found to be more sensitive, shown by a smaller value of P as tabulated in Table 3. The selected ten out of seventeen parameters, which vigorously govern the rainfall-runoff process, are listed in Table 4.

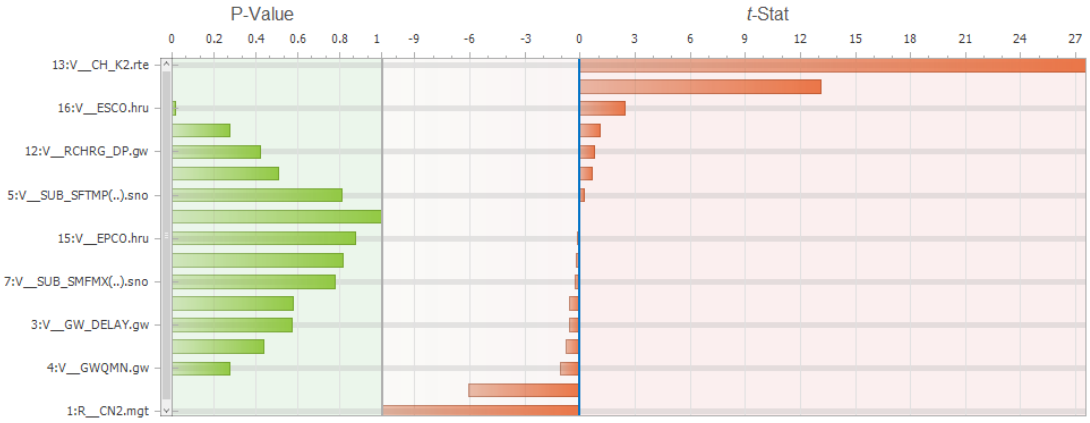

Figure 7. Model sensitive parameters of the study catchment.

Table 3. Parameter sensitivity analysis.

Parameter Name	Definition	*t*-Stat	*p*-Value
r__CN2.mgt	SCS curve number	−10.751	0.000
v__ALPHA_BF.gw	Base flow factor	−6.063	0.000
v__GWQMN.gw	Threshold depth of water in the shallow aquifer for return flow to occur (mm H_2O)	−1.089	0.276
v__SUB_SMTMP(..).sno	Snowmelt base temperature	−0.776	0.438
v__GW_DELAY.gw	Groundwater delay	−0.567	0.571
v__GW_REVAP.gw	Groundwater revap coefficient	−0.558	0.577
v__SUB_SMFMX(..).sno	Maximum melt rate for snow during year (mm H_2O/°C/day)	−0.279	0.780
v__SUB_SMFMN(..).sno	Annual minimum melt rate for snow	−0.231	0.817
v__EPCO.hru	Plant uptake compensation factor	−0.158	0.875
r__SOL_AWC(..).sol	Available water capacity of soil layer	0.000	1.000
v__SUB_SFTMP(..).sno	Snowfall temperature	0.242	0.809
v__REVAPMN.gw	Threshold depth of water in the shallow aquifer for "revap" to occur (mm H_2O)	0.658	0.510
v__RCHRG_DP.gw	Deep aquifer percolation fraction	0.799	0.424
v__SUB_TIMP(..).sno	Snow temperature lag factor	1.093	0.275
v__ESCO.hru	Soil evaporation compensation factor	2.426	0.015
v__CH_N2.rte	Manning's "n" value for the channel	13.114	0.000
v__CH_K2.rte	Effective hydraulic conductivity of channel	27.547	0.000

Table 4. Initial and optimized sensitive parameter ranges during calibration of daily IMERG-F.

Sr.	Parameters	Initial Parameters Ranges		Optimized Parameters Ranges	
		Lower Limit	Upper Limit	Lower Limit	Upper Limit
1	v__ALPHA_BF.gw	0	1	0	0.65
2	v__GW_DELAY.gw	0	500	145.20	435.79
3	v__REVAPMN.gw	0	500	218.19	654.80
4	v__GW_REVAP.gw	0.02	0.2	0.02	0.11
5	v__SUB_SMTMP().sno	−5	5	−5	0.18
6	v__SUB_SFTMP().sno	−5	5	−4.34	1.89
7	r__CN2.mgt	−0.25	0.25	0.24	0.25
8	v__CH_K2.rte	0.001	200	55.08	165.32
9	v__CH_N2.rte	−0.01	0.3	0.107	0.3
10	v__ESCO.hru	0	1	0.474	1.42

4.3. Calibration and Validation

After GSA, calibration was done with ten sensitive parameters by running 500 simulations in three iterations. A single iteration for validation was carried out by selecting a similar number of simulations as in the last iteration of the calibration.

4.4. Performance Indices

Two indices—P-factor and R-factor—were introduced in SWAT-CUP to quantify the prediction uncertainties [53]. The P-factor is the percentage of observed data bracketed by a 95% prediction boundary often known as 95 % prediction uncertainty, or 95PPU. Its value ranges from 0 to 1, in which a value close to 1 depicts the very high model performance and agrees the 100% enveloping of the observed data within the model prediction uncertainty. The R-factor denotes the thickness of the 95PPU envelope and varies in the range 0–1 [54]. P and R factors are closely linked to each other, which indicates that a higher value of P-factor can be achieved with the expense of the higher value of the R-factor. The best-calibrated ranges can be achieved by balancing in P and R factor values. For calibration of discharge, the P-factor value greater than 0.7 and R-factor value less than 1.5 is acceptable [74].

Coefficient of determination (R^2) and the Nash–Sutcliffe efficiency (NSE) [75] were used to indicate the goodness of fit for the best simulation. R^2 depicts the strength of linear correlation between observed and simulated discharge values and its value stretches from 0 to 1. The best model performance is indicated by a value close to 1 and a value greater than 0.5 is considered acceptable [76]. NSE defines how perfectly the observed and simulated data match the 1:1 line [77]. Its value lies in $-\infty$ to 1. Moriasi et al. [76] classified the model performance using NSE value: unsatisfactory performance ($NSE \leq 0.50$), satisfactory performance ($0.50 \leq NSE \leq 0.65$), good performance ($0.65 \leq NSE \leq 0.75$) and very good performance ($0.75 \leq NSE \leq 1.00$).

PBIAS tends to capture the underestimation or overestimation of simulated values from observed values. PBIAS has 0 value under optimal conditions, whereas a positive value shows an underestimation of the prediction and negative value depicts that the model overestimates the prediction [78]. Van Liew et al. [79] classified PBIAS values into three classes: good at ±20%, satisfactory between ±20% and ±40% and unsatisfactory at ±40%.

5. Results

5.1. Calibration and Validation of the SWAT Model

The list of ten sensitive parameters with their initial and optimized ranges, obtained in the calibration of daily IMERG-F model, are tabulated in Table 4. These ten parameters, with their initial parameters' ranges, were further used in the calibration of other models. Eckhardt et al. [80] described that the range of parameters in the calibration process should be in physically permissible limits. Optimized parameter ranges were obtained by running three iterations of 500 simulations each. To identify the best parameter ranges for simulation, Nash–Sutcliff efficiency (NSE) was selected as an objective function due to its extensive use in hydrologic modeling [81].

Calibration and validation are very important aspects of hydrological modeling. In the calibration phase, model parameters are tuned enough to get good agreement between observed and simulated values. Further, these tuned parameters are validated for the next period. The fitted values of tuned parameters used in the calibration and validation of the model are given in Table 5. In this study, daily time series data of six years (2001–2006), including the initial warmup period of two years (2001–2002), were used for calibration of the model while the model was further validated for the next four years (2007–2010). Moreover, the model was also calibrated and validated on a monthly timescale for the same duration.

Table 5. Fitted parameter values of IMERG-F and 3B42.

Sr.	Parameters	Fitted Parameter Values			
		IMERG-F		3B42	
		Daily	Monthly	Daily	Monthly
1	v__ALPHA_BF.gw	0.26	0.22	0.21	0.52
2	v__GW_DELAY.gw	184.43	334.96	314.04	320.43
3	v__REVAPMN.gw	425.58	585.38	599.35	475.36
4	v__GW_REVAP.gw	0.02	0.02	0.02	0.04
5	v__SUB_SMTMP().sno	−3.22	−1.46	−4.82	−1.07
6	v__SUB_SFTMP().sno	−1.07	−2.08	−2.00	0.13
7	r__CN2.mgt	0.25	0.24	0.25	0.23
8	v__CH_K2.rte	131.48	103.48	115.82	160.14
9	v__CH_N2.rte	0.25	0.17	0.29	0.21
10	v__ESCO.hru	1.32	1.05	1.38	1.32

5.2. Runoff Simulation on Daily and Monthly Timescale

To check the detectability of satellite precipitation products, two types of products were used in the SWAT model to simulate the runoff at the Marala Barrage gauging site in River Chenab. The model was set up with a daily GPM product (IMERG-F) and a daily TRMM product (3B42). It was then calibrated using the SWAT-CUP model in the SUFI-2 algorithm. Calibrated and validated outputs of IMERG-F and 3B42 on daily timescale are shown in Figure 8. The calibration range in Figure 8 is 2003–2006 and the validation range is 2007–2010. Calibrated and validated hydrographs show that both satellite precipitation products have less tendency to capture peaks, whereas low flows are well captured in the model. It is observed in the peak of the validation period in 2009 that the IMERG-F product captures a peak more precisely than the 3B42 product. Five kinds of evaluation indices (P-factor, R-factor, R^2, NSE and PBIAS) were used to evaluate the detection precision of IMERG-F and 3B42 as depicted in Figure 9. For best flow model calibration, values of P-factor and R-factor should be greater than 0.7 and less than 1.5, respectively. According to Figure 9a,b, the values of the P-factor and R-factor are within acceptable limits for IMERG-F and 3B42 products. The results of R^2 show that IMERG-F has outperformed the 3B42 (Figure 9c), where calibration of IMERG-F and 3B42 displays 0.61 and 0.57 while validation displays 0.66 and 0.64, respectively. A similar trend for NSE is noted in Figure 9d, where calibration of IMERG-F and 3B42 exhibit 0.54 and 0.45, while for validation the values are 0.61 and 0.54, respectively. Figure 9e shows that the SWAT model driven by daily IMERG-F precipitation produces a moderate underestimate of 22.8% in calibration and 21.5% in validation, whereas 3B42 data produces extreme underestimation of 30.9% in calibration and 31.1% in validation. From the above discussion, the daily IMERG-F appears to be a little more favorable than the daily 3B42 precipitation product in an ungauged Chenab River catchment.

In the case of monthly aggregated flows from daily flows, the model results are fairly in line with the observed monthly flows (Figure 10). There is a significant improvement in the performance of both IMERG-F and 3B42 products compared to the daily timescale. As on the daily timescale, the model is unable to capture the peak flows, whereas, on a monthly timescale, model performance in capturing the peaks is very accurate. However, results produced by IMERG-F are still better than 3B42 on a monthly scale. In terms of R^2 and NSE, both IMERG-F and 3B42 exhibit higher values on a monthly timescale than a daily timescale. The accumulated monthly simulated flows using IMERG-F produces best-simulated results with R^2 of 0.86 and 0.89, NSE of 0.77 and 0.82 for calibration and validation, respectively (Figure 9c,d). The statistical comparison for both products on a monthly scale is also displayed in Figure 9. However, the ability of both satellite products to capture the peak flows is lower,

but overall, the IMERG-F performed better than 3B42. Therefore, by observing the statistical indices of both satellite products, the IMERG-F is considered to be a perfect replacement for the 3B42 for an ungauged Chenab River catchment.

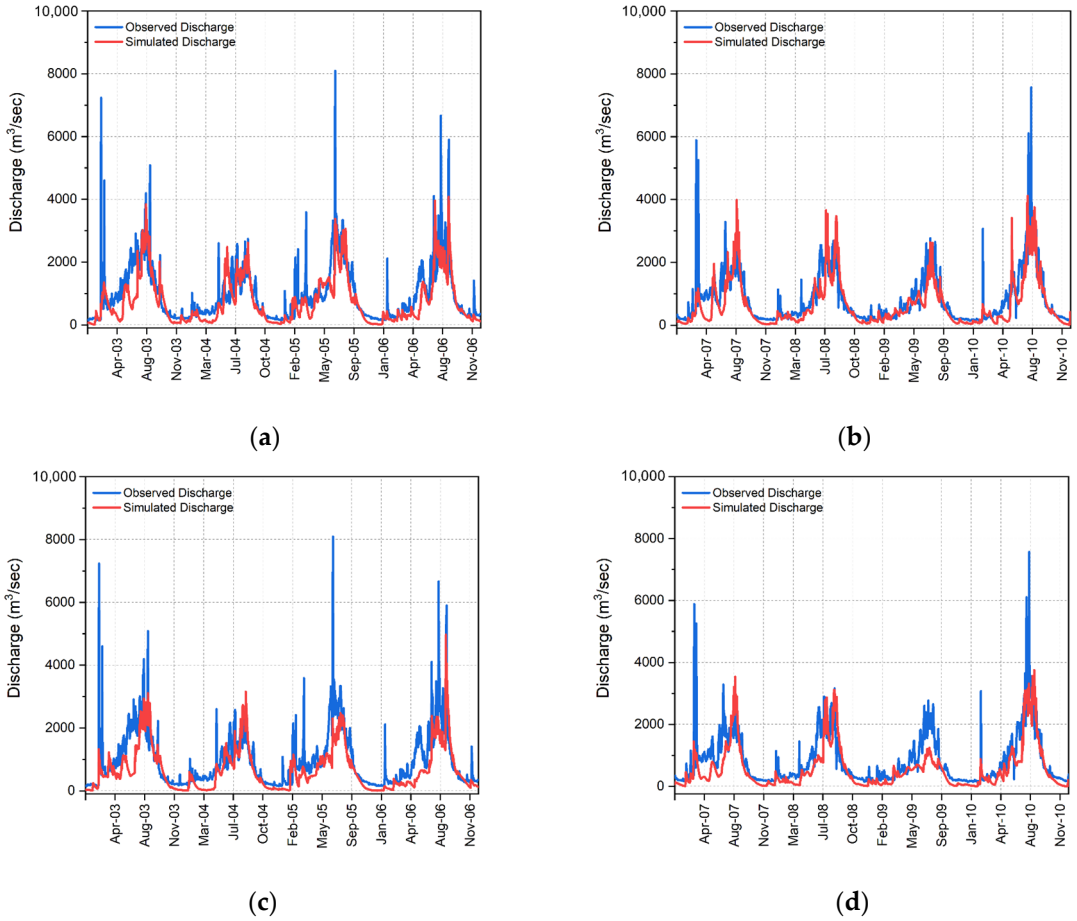

Figure 8. Hydrographs between daily observed and simulated flows (**a**) IMERG-F calibration (**b**) IMERG-F validation (**c**) 3B42 calibration (**d**) 3B42 validation.

5.3. Taylor Diagrams

Taylor diagrams were plotted to concise the statistical summary on how well satellite-based simulated discharge agrees with the observed discharge at the Marala Barrage gauging site (Figure 11). Taylor [82] has constructed a significant diagram by plotting the standard deviation of the time series of the simulated values and the Pearson correlation between the time series of simulated and observed values. He also realized the connection between standard deviation, correlation and the centered pattern Root Mean Square (RMS) error difference and found that they can be displayed in a single diagram. In Taylor diagram, the RMS error in simulated discharge is related to the distance from the "observed" point on the x-axis, the correlation (similarity between simulated and observed discharges) is proportional to the azimuthal angle, and the standard deviation of simulated discharges is related to the radial distance from the origin. Model simulations will be considered as best fit with the observed discharge when it will lie near to the point marked "Observed" on the x-axis.

Figure 11 indicates that among both satellite precipitation products, IMERG-F and 3B42, the IMERG-F-based model run provides the best approximation to the time series of observed discharge. However, 3B42 driven simulation run is satisfactory comparable to observed discharge. The overall hydrologic model performance at monthly and daily scale is depicted in Figure 11, where the blue square represents the 3B42 product and the red triangle represents the IMERG-F. It is evident from Figure 11a,b that at daily timescale, the value of R is between 0.76–0.81, and the RMS error value is

between 506.22–655.54 m^3/sec. In contrast, at a monthly scale (Figure 11c,d), the value of R is between 0.90–0.94, and the RMS error value is in between 295.71–445.11 m^3/sec. This trend depicts that the results from monthly simulations dominate results from daily simulations. Nevertheless, IMERG-F performs better than 3B42 on both monthly and daily timescale. The monthly 3B42-based model run obtained lower R (calibration, 0.90 and validation, 0.92) and higher RMS errors (calibration, 445.11 m^3/s and validation, 373.81 m^3/s) than the monthly IMERGE-F-based model run with R (calibration, 0.93 and validation, 0.94) and RMS errors (calibration, 357.88 m^3/s and validation, 295.71 m^3/s) (Figure 11c,d). The best simulation in all model runs is from monthly IMERG-F with a higher value of R and less RMS error.

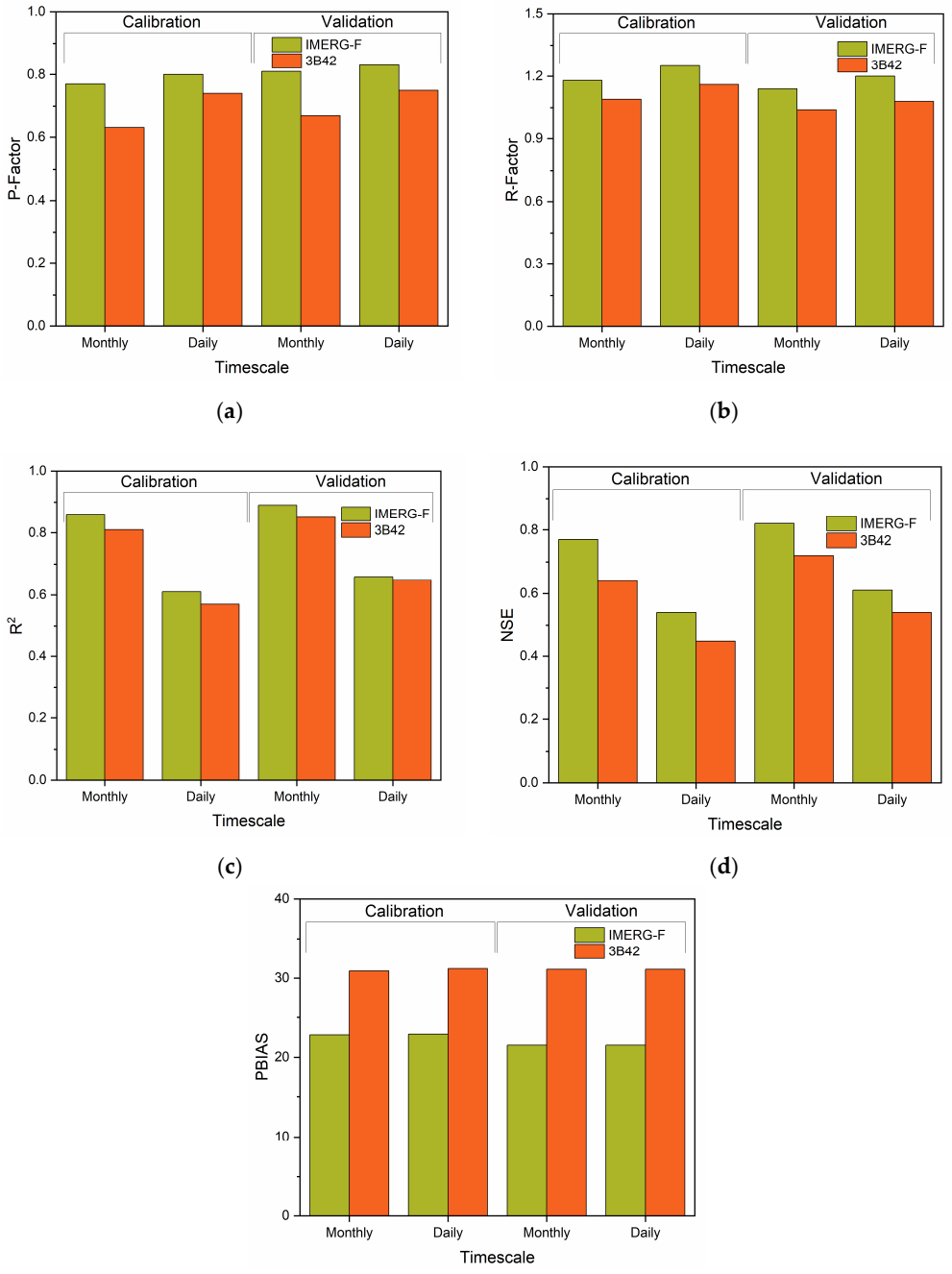

Figure 9. Model evaluation indices for calibration '2003–2006' and validation '2007–2010' period on monthly and daily timescale (**a**) P-Factor (**b**) R-Factor (**c**) R^2 (**d**) NSE (**e**) PBIAS.

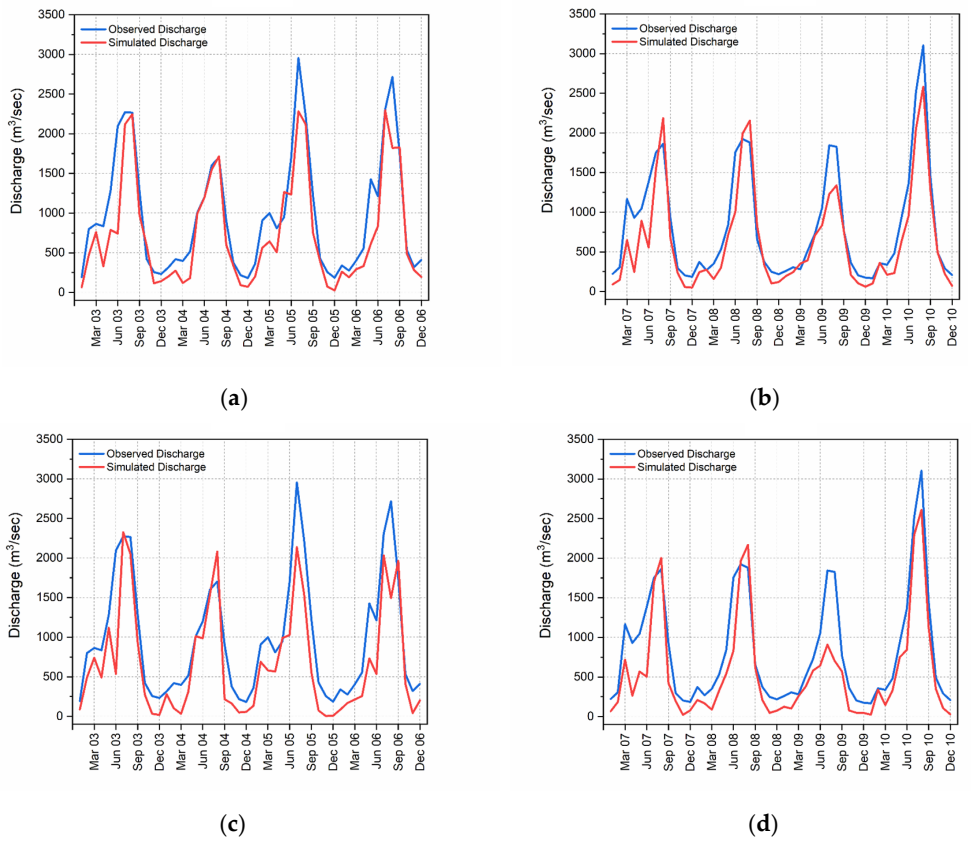

Figure 10. Hydrographs between monthly observed and simulated flows (**a**) IMERG-F calibration (**b**) IMERG-F validation (**c**) 3B42 calibration (**d**) 3B42 validation.

The comparison between simulated discharges from IMERG-F and 3B42 shows that IMERG-F is the best precipitation input for the Chenab River catchment. The simulated flow from IMERG-F is more in agreement with the observed flow and has much better values of performance indices than 3B42. This tendency is similar for daily and monthly timescale. This study is useful for the ungauged Chenab River catchment where data sharing is very insufficient from the Indian side catchment. In this situation, satellite-based precipitation estimates would bring significant results for rainfall-runoff modeling for this river. The overall complete performance indices of calibration and validation stages of IMERG-F and 3B42 are given in Tables A1 and A2.

6. Summary, Conclusions and Recommendations

6.1. Summary

The main objective of this study was to choose the feasible satellite precipitation product from two renowned products, i.e., GPM IMERG-F version 6 and TRMM 3B42 version 7, for reliable hydrological modeling in the ungauged catchment of Chenab River in Pakistan. The physical-based semidistributed hydrological model of SWAT was selected to simulate the runoff in the catchment. To evaluate the prediction uncertainties, Abbaspour et al. [74] recommended that the values of the P-factor should be greater than 0.7 and the value of R-Factor should be less than 1.5 for calibration of discharges. For all calibrated and validated events, the value of P-Factor is greater than 0.77 for IMERG-F and greater than 0.63 for 3B42. The range of R-Factor is between 1.14–1.25 and 1.04–1.16 for IMERG-F and 3B42, respectively. To evaluate the performance of satellite precipitation products, three main statistical indices, R^2, NSE and PBIAS, were considered. The simulated results for daily 3B42 show a lower resemblance to daily observed discharges with R^2 (0.57 Calibration, 0.64 Validation) and NSE (0.45 Calibration, 0.54 Validation). The daily IMERG-F gives a satisfactory performance with R^2

(0.61 Calibration, 0.66 Validation) and NSE (0.54 Calibration, 0.61 Validation). A model performance with accumulated monthly flows from satellite precipitation products shows a significant improvement, which indicates a better agreement with observed hydrographs in both calibration and validation phases. IMERG-F input yields the best model performance at monthly timescale with R^2 of 0.86 and 0.89 and NSE of 0.77 and 0.82 for calibration and validation, respectively. The monthly output of 3B42 is also satisfactory with R^2 of 0.81 and 0.85 and NSE of 0.64 and 0.72 for calibration and validation, respectively. Both satellite products underestimate the discharges at daily and monthly scale. However, 3B42 produces more underestimation with PBIAS (30.9 Calibration, 31.1 Validation) than IMERG-F with PBIAS (22.8 Calibration, 21.5 Validation). The retrieved results from the Taylor diagram depicted that IMERG-F outperformed the 3B42 precipitation with higher values of R and lower RMS error (Table A2).

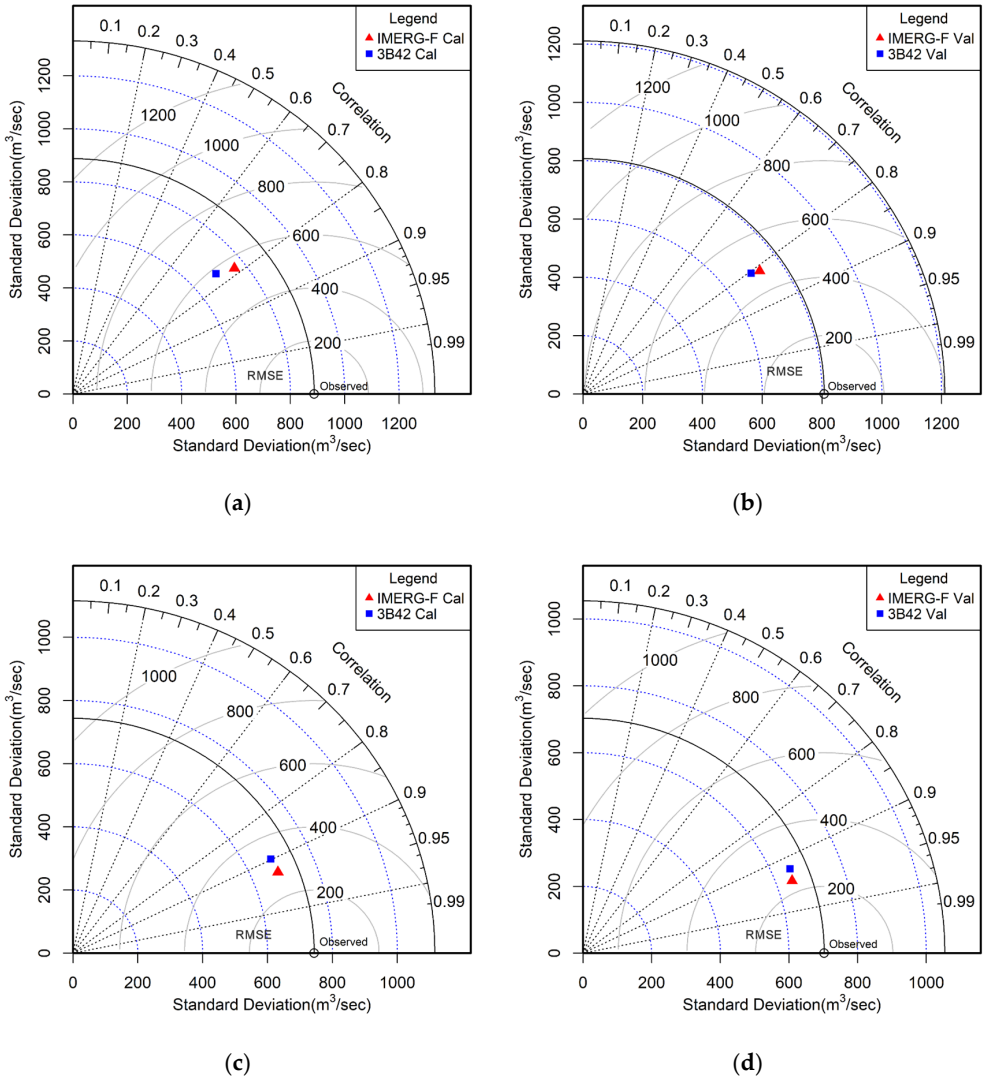

Figure 11. Taylor diagrams showing the comparison of the IMERG-F and 3B42 at Marala Barrage gauging site with respect to the stream gauge observations (**a**) daily calibration (**b**) daily validation (**c**) monthly calibration (**d**) monthly validation.

6.2. Conclusions

In comparison to daily timescale simulations, the performance of IMERG-F v6 and 3B42 v7 depicted that discharge simulation at a monthly timescale has higher values of R^2, NSE and R, while values of PBIAS and RMS error are lower. Moreover, from the comparison between IMERG-F v6

and 3B42 v7, it was observed that the performance of IMERG-F v6 was more favorable than 3B42 v7 by indicating higher R^2, NSE and R values and lower PBIAS and RMS error at both monthly and daily timescale. Therefore, GPM IMERG-F v6 is identified as a potential replacement for TRMM 3B42 v7 product at the Chenab River catchment.

6.3. Recommendations

Overall, this study demonstrates that satellite precipitation products are a valuable source of rainfall data and provide useful input for hydrological simulation in the ungauged Chenab River catchment. These results could encourage water managers to choose satellite precipitation products for runoff modeling in this catchment or nearby similar catchments in the future. This research was only accomplished by using only two open-source satellite precipitation products, while there are many other open-source precipitation products are available. Moreover, climatic data like temperature, wind speed, solar radiation and evaporation can be accessed from other open-source platforms. This means that the use of open-source data for hydrologic simulation in ungauged catchments is worth studying.

Author Contributions: Conceptualization, E.A.; methodology, E.A.; software, E.A. and N.S.; validation, E.A. and N.S.; data curation, E.A. and W.Y.; writing—original draft preparation, E.A.; writing—review and editing, J.Z.; visualization, F.A.J.; supervision, P.K. All authors have read and agreed to the published version of the manuscript.

Funding: This research received no external funding.

Acknowledgments: E.A. is thankful to the Higher Education Commission of Pakistan (HEC) and German Academic Exchange Service (DAAD) for providing him the opportunity to carry out his Ph.D. studies in Germany. Authors would like to say thanks to flood forecasting division, Pakistan Meteorological Department, (PMD) for providing useful data to conduct this research. Institute of Urban and Industrial Water Management, TU Dresden facilitated E.A. to conduct this research. E.A. would also like to thank Technische Universität Dresden for open access publication fund.

Conflicts of Interest: The authors declare no conflicts of interests.

Appendix A

Table A1. Performance indices results of calibration (2003–2006) and validation (2007–2010).

Satellite Precipitation Product	Calibration/Validation	Timescale	P-factor	R-factor	R^2	NSE	PBIAS
IMERG-F	Calibration	Monthly	0.77	1.18	0.86	0.77	22.8
	Validation		0.81	1.14	0.89	0.82	21.5
	Calibration	Daily	0.80	1.25	0.61	0.54	22.8
	Validation		0.83	1.20	0.66	0.61	21.5
3B42	Calibration	Monthly	0.63	1.09	0.81	0.64	30.9
	Validation		0.67	1.04	0.85	0.72	31.1
	Calibration	Daily	0.74	1.16	0.57	0.45	30.9
	Validation		0.75	1.08	0.65	0.54	31.1

Table A2. Taylor diagram statics of model for calibration (2003–2006) and validation (2007–2010).

Statistics	Satellite Precipitation Product	Monthly		Daily	
		Calibration	Validation	Calibration	Validation
R	IMERG-F	0.93	0.94	0.78	0.81
	3B42	0.90	0.92	0.76	0.81
RMS error	IMERG-F	357.88	295.71	601.61	506.22
	3B42	445.11	373.81	655.54	545.90
Standard Deviation	IMERG-F	722.13	681.06	834.12	772.86
	3B42	727.80	690.71	811.47	765.67

References

1. Huffman, G.J.; Adler, R.F.; Bolvin, D.T.; Gu, G.; Nelkin, E.J.; Bowman, K.P.; Hong, Y.; Stocker, E.F.; Wolff, D.B. The TRMM Multisatellite Precipitation Analysis (TMPA): Quasi-Global, multiyear, combined-sensor precipitation estimates at fine scales. *J. Hydrometeorol.* **2007**, *8*, 38–55. [CrossRef]
2. Hou, A.Y.; Kakar, R.K.; Neeck, S.; Azarbarzin, A.A.; Kummerow, C.D.; Kojima, M.; Oki, R.; Nakamura, K.; Iguchi, T. The Global precipitation measurement mission. *Bull. Am. Meteorol. Soc.* **2014**, *95*, 701–722. [CrossRef]
3. Saddique, N.; Usman, M.; Bernhofer, C. Simulating the impact of climate change on the hydrological regimes of a sparsely gauged mountainous basin, Northern Pakistan. *Water (Switzerland)* **2019**, *11*, 2141. [CrossRef]
4. Miyamoto, M.; Ono, M.; Okazumi, T.; Nabesaka, S.; Iwami, Y. Applicability of a Flood Forecasting Method utilizing Global Satellite Information to an Insufficiently-Gauged River Basin: A Case of a River Basin in the Philippines. In Proceedings of the 11th International Conference on Hydroinformatics HIC 2014, New York City, NY, USA, 17–21 August 2014.
5. Boongaling, C.G.K.; Faustino-Eslava, D.V.; Lansigan, F.P. Modeling land use change impacts on hydrology and the use of landscape metrics as tools for watershed management: The case of an ungauged catchment in the Philippines. *Land Use Policy* **2018**, *72*, 116–128. [CrossRef]
6. Jodar-Abellan, A.; Valdes-Abellan, J.; Pla, C.; Gomariz-Castillo, F. Impact of land use changes on flash flood prediction using a sub-daily SWAT model in five Mediterranean ungauged watersheds (SE Spain). *Sci. Total Environ.* **2019**, *657*, 1578–1591. [CrossRef]
7. Dash, P. Simulation of Hydrologic Processes through Calibration of SWAT Model with MODIS Evapotranspiration Data for an Ungauged Basin in Western Himalaya, India. In *Geospatial Applications for Natural Resources Management*; CRC Press: Boca Raton, FL, USA, 2018; pp. 223–241.
8. Wu, Y.; Zhang, Z.; Huang, Y.; Jin, Q.; Chen, X.; Chang, J. Evaluation of the GPM IMERG v5 and TRMM 3B42 v7 precipitation products in the Yangtze River basin, China. *Water (Switzerland)* **2019**, *11*, 1459. [CrossRef]
9. Yuan, F.; Zhang, L.; Soe, K.M.W.; Ren, L.; Zhao, C.; Zhu, Y.; Jiang, S.; Liu, Y. Applications of TRMM- and GPM-era multiple- satellite precipitation products for flood simulations at sub-daily scales in a sparsely gauged watershed in Myanmar. *Remote Sens.* **2019**, *11*, 140. [CrossRef]
10. Nguyen, T.; Masih, I.; Mohamed, Y.; Van Der Zaag, P. Validating Rainfall-Runoff Modelling Using Satellite-Based and Reanalysis Precipitation Products in the Sre Pok Catchment, the Mekong River Basin. *Geosciences* **2018**, *8*, 164. [CrossRef]
11. Qureshi, A.S. Water Management in the Indus Basin in Pakistan: Challenges and Opportunities. *Mt. Res. Dev.* **2011**, *31*, 252–260. [CrossRef]
12. Rees, H.G.; Collins, D.N. Regional differences in response of flow in glacier-fed Himalayan rivers to climatic warming. *Hydrol. Process.* **2006**, *20*, 2157–2169. [CrossRef]
13. Riaz, M.; Aziz, A.; Hussain, S. Flood Forecasting of an ungauged trans-boundary chenab river basin using distributed hydrological model Integrated Flood Analysis System (IFAS). *Pak. J. Meteorol.* **2017**, *13*, 51–62.
14. FFC. *Annual Flood Report For the Year 2012*; Federal Flood Commision, Govt. of Pakistan: Islamabad, Pakistan, 2013.
15. Tarnavsky, E.; Mulligan, M.; Ouessar, M.; Faye, A.; Black, E. Dynamic Hydrological Modeling in Drylands with TRMM Based Rainfall. *Remote Sens.* **2013**, *5*, 6691. [CrossRef]
16. Yoshimoto, S.; Amarnath, G. Applications of Satellite-Based Rainfall Estimates in Flood Inundation Modeling—A Case Study in Mundeni Aru River Basin, Sri Lanka. *Remote Sens.* **2017**, *9*, 998. [CrossRef]
17. Tuo, Y.; Duan, Z.; Disse, M.; Chiogna, G. Evaluation of precipitation input for SWAT modeling in Alpine catchment: A case study in the Adige river basin (Italy). *Sci. Total Environ.* **2016**, *573*, 66–82. [CrossRef]
18. Qi, W.; Zhang, C.; Fu, G.; Sweetapple, C.; Zhou, H. Evaluation of global fine-resolution precipitation products and their uncertainty quantification in ensemble discharge simulations. *Hydrol. Earth Syst. Sci.* **2016**, *20*, 903–920. [CrossRef]
19. Xue, X.; Hong, Y.; Limaye, A.S.; Gourley, J.J.; Huffman, G.J.; Khan, S.I.; Dorji, C.; Chen, S. Statistical and hydrological evaluation of TRMM-based Multi-satellite Precipitation Analysis over the Wangchu Basin of Bhutan: Are the latest satellite precipitation products 3B42V7 ready for use in ungauged basins? *J. Hydrol.* **2013**, *499*, 91–99. [CrossRef]
20. Saber, M.; Yilmaz, K. Evaluation and Bias Correction of Satellite-Based Rainfall Estimates for Modelling Flash Floods over the Mediterranean region: Application to Karpuz River Basin, Turkey. *Water (Switzerland)* **2018**, *10*, 657. [CrossRef]

21. Gebremichael, M.; Hossain, F. *Satellite Rainfall Applications for Surface Hydrology*; Gebremichael, M., Hossain, F., Eds.; Springer: Dordrecht, The Netherlands, 2010; ISBN 978-90-481-2914-0.
22. Tobin, K.J.; Bennett, M.E. Temporal analysis of Soil and Water Assessment Tool (SWAT) performance based on remotely sensed precipitation products. *Hydrol. Process.* **2013**, *27*, 505–514. [CrossRef]
23. Wang, Z.; Zhong, R.; Lai, C.; Chen, J. Evaluation of the GPM IMERG satellite-based precipitation products and the hydrological utility. *Atmos. Res.* **2017**, *196*, 151–163. [CrossRef]
24. Jiang, S.; Ren, L.; Xu, C.Y.; Yong, B.; Yuan, F.; Liu, Y.; Yang, X.; Zeng, X. Statistical and hydrological evaluation of the latest Integrated Multi-satellitE Retrievals for GPM (IMERG) over a midlatitude humid basin in South China. *Atmos. Res.* **2018**, *214*, 418–429. [CrossRef]
25. Huffman, G.J.; Bolvin, D.T.; Braithwaite, D.; Hsu, K.-L.; Joyce, R.J.; Kidd, C.; Nelkin, E.J.; Sorooshian, S.; Stocker, E.F.; Tan, J.; et al. Integrated multi-satellite retrievals for the Global Precipitation Measurement (GPM) Mission (IMERG). In *Satellite Precipitation Measurement*; Springer: Cham, Germany, 2020; pp. 343–353. [CrossRef]
26. Prakash, S.; Mitra, A.K.; AghaKouchak, A.; Liu, Z.; Norouzi, H.; Pai, D.S. A preliminary assessment of GPM-based multi-satellite precipitation estimates over a monsoon dominated region. *J. Hydrol.* **2018**, *556*, 865–876. [CrossRef]
27. Khodadoust Siuki, S.; Saghafian, B.; Moazami, S. Comprehensive evaluation of 3-hourly TRMM and half-hourly GPM-IMERG satellite precipitation products. *Int. J. Remote Sens.* **2017**, *38*, 558–571. [CrossRef]
28. Kim, K.; Park, J.; Baik, J.; Choi, M. Evaluation of topographical and seasonal feature using GPM IMERG and TRMM 3B42 over Far-East Asia. *Atmos. Res.* **2017**, *187*, 95–105. [CrossRef]
29. Tang, G.; Ma, Y.; Long, D.; Zhong, L.; Hong, Y. Evaluation of GPM Day-1 IMERG and TMPA Version-7 legacy products over Mainland China at multiple spatiotemporal scales. *J. Hydrol.* **2016**, *533*, 152–167. [CrossRef]
30. Gebregiorgis, A.S.; Kirstetter, P.; Hong, Y.E.; Gourley, J.J.; Huffman, G.J.; Petersen, W.A.; Xue, X.; Schwaller, M.R. To What Extent is the Day 1 GPM IMERG Satellite precipitation estimate improved as compared to TRMM TMPA-RT? *J. Geophys. Res. Atmos.* **2018**, *123*, 1694–1707. [CrossRef]
31. Anjum, M.N.; Ding, Y.; Shangguan, D.; Ahmad, I.; Ijaz, M.W.; Farid, H.U.; Yagoub, Y.E.; Zaman, M.; Adnan, M. Performance evaluation of latest integrated multi-satellite retrievals for Global Precipitation Measurement (IMERG) over the northern highlands of Pakistan. *Atmos. Res.* **2018**, *205*, 134–146. [CrossRef]
32. Rozante, J.; Vila, D.; Barboza Chiquetto, J.; Fernandes, A.; Souza Alvim, D. Evaluation of TRMM/GPM blended daily products over Brazil. *Remote Sens.* **2018**, *10*, 882. [CrossRef]
33. Tan, M.L.; Santo, H. Comparison of GPM IMERG, TMPA 3B42 and PERSIANN-CDR satellite precipitation products over Malaysia. *Atmos. Res.* **2018**, *202*, 63–76. [CrossRef]
34. Prakash, S.; Mitra, A.K.; Pai, D.S.; AghaKouchak, A. From TRMM to GPM: How well can heavy rainfall be detected from space? *Adv. Water Resour.* **2016**, *88*, 1–7. [CrossRef]
35. Sharifi, E.; Steinacker, R.; Saghafian, B. Assessment of GPM-IMERG and other precipitation products against gauge data under different topographic and climatic conditions in Iran: Preliminary results. *Remote Sens.* **2016**, *8*, 135. [CrossRef]
36. He, Z.; Yang, L.; Tian, F.; Ni, G.; Hou, A.; Lu, H. Intercomparisons of Rainfall Estimates from TRMM and GPM Multisatellite products over the upper Mekong River Basin. *J. Hydrometeorol.* **2017**, *18*, 413–430. [CrossRef]
37. Zubieta, R.; Getirana, A.; Espinoza, J.C.; Lavado-Casimiro, W.; Aragon, L. Hydrological modeling of the Peruvian–Ecuadorian Amazon Basin using GPM-IMERG satellite-based precipitation dataset. *Hydrol. Earth Syst. Sci.* **2017**, *21*, 3543–3555. [CrossRef]
38. Yuan, F.; Wang, B.; Shi, C.; Cui, W.; Zhao, C.; Liu, Y.; Ren, L.; Zhang, L.; Zhu, Y.; Chen, T.; et al. Evaluation of hydrological utility of IMERG Final run V05 and TMPA 3B42V7 satellite precipitation products in the Yellow River source region, China. *J. Hydrol.* **2018**, *567*, 696–711. [CrossRef]
39. Arnold, J.G.; Fohrer, N. SWAT2000: Current capabilities and research opportunities in applied watershed modelling. *Hydrol. Process.* **2005**, *19*, 563–572. [CrossRef]
40. Arnold, J.G.; Srinivasan, R.; Muttiah, R.S.; Williams, J.R. Large area hydrologic modeling and assessment part I: Model development. *J. Am. Water Resour. Assoc.* **1998**, *34*, 73–89. [CrossRef]
41. Nerantzaki, S.D.; Giannakis, G.V.; Efstathiou, D.; Nikolaidis, N.P.; Sibetheros, I.A.; Karatzas, G.P.; Zacharias, I. Modeling suspended sediment transport and assessing the impacts of climate change in a karstic Mediterranean watershed. *Sci. Total Environ.* **2015**, *538*, 288–297. [CrossRef]

42. Schmalz, B.; Kuemmerlen, M.; Kiesel, J.; Cai, Q.; Jähnig, S.C.; Fohrer, N. Impacts of land use changes on hydrological components and macroinvertebrate distributions in the Poyang lake area. *Ecohydrology* **2015**, *8*, 1119–1136. [CrossRef]
43. Song, X.; Duan, Z.; Kono, Y.; Wang, M. Integration of remotely sensed C factor into SWAT for modelling sediment yield. *Hydrol. Process.* **2011**, *25*, 3387–3398. [CrossRef]
44. Guse, B.; Pfannerstill, M.; Strauch, M.; Reusser, D.E.; Lüdtke, S.; Volk, M.; Gupta, H.; Fohrer, N. On characterizing the temporal dominance patterns of model parameters and processes. *Hydrol. Process.* **2016**, *30*, 2255–2270. [CrossRef]
45. Chen, W.; Chau, K.W. Intelligent manipulation and calibration of parameters for hydrological models. *Int. J. Environ. Pollut.* **2006**, *28*, 432–447. [CrossRef]
46. Woznicki, S.A.; Nejadhashemi, A.P.; Abouali, M.; Herman, M.R.; Esfahanian, E.; Hamaamin, Y.A.; Zhang, Z. Ecohydrological modeling for large-scale environmental impact assessment. *Sci. Total Environ.* **2016**, *543*, 274–286. [CrossRef] [PubMed]
47. Rahman, K.; Maringanti, C.; Beniston, M.; Widmer, F.; Abbaspour, K.; Lehmann, A. Streamflow modeling in a highly managed mountainous glacier watershed using SWAT: The upper rhone river watershed case in Switzerland. *Water Resour. Manag.* **2013**, *27*, 323–339. [CrossRef]
48. Guo, H.; Hu, Q.; Jiang, T. Annual and seasonal streamflow responses to climate and land-cover changes in the Poyang Lake basin, China. *J. Hydrol.* **2008**, *355*, 106–122. [CrossRef]
49. Ayana, E.K.; Worqlul, A.W.; Steenhuis, T.S. Evaluation of stream water quality data generated from MODIS images in modeling total suspended solid emission to a freshwater lake. *Sci. Total Environ.* **2015**, *523*, 170–177. [CrossRef]
50. Abbaspour, K.C. SWAT-CUP 2012: SWAT Calibration and Uncertainty Programs - A User Manual 1012. *Eawag–Swiss Fed. Inst. Aquat. Sci. Technol.* 2015. Available online: https://swat.tamu.edu/media/114860/usermanual_swatcup.pdf (accessed on 12 May 2020).
51. Zheng, Y.; Keller, A.A. Uncertainty assessment in watershed-scale water quality modeling and management: 1. Framework and application of generalized likelihood uncertainty estimation (GLUE) approach. *Water Resour. Res.* **2007**, *43*, 1–13. [CrossRef]
52. Yang, J.; Reichert, P.; Abbaspour, K.C.; Xia, J.; Yang, H. Comparing uncertainty analysis techniques for a SWAT application to the Chaohe Basin in China. *J. Hydrol.* **2008**, *358*, 1–23. [CrossRef]
53. Abbaspour, K.C.; Johnson, C.A.; Van Genuchten, M.T. Estimating Uncertain Flow and Transport Parameters Using a Sequential Uncertainty Fitting Procedure. *Vadose Zone J.* **2004**, *3*, 1340–1352. [CrossRef]
54. Abbaspour, K.C.; Yang, J.; Maximov, I.; Siber, R.; Bogner, K.; Mieleitner, J.; Zobrist, J.; Srinivasan, R. Modelling hydrology and water quality in the pre-alpine/alpine Thur watershed using SWAT. *J. Hydrol.* **2007**, *333*, 413–430. [CrossRef]
55. Beven, K.; Binley, A. The future of distributed models: Model calibration and uncertainty prediction. *Hydrol. Process.* **1992**, *6*, 279–298. [CrossRef]
56. Van Griensven, A.; Meixner, T. Methods to quantify and identify the sources of uncertainty for river basin water quality models. *Water Sci. Technol.* **2006**, *53*, 51–59. [CrossRef]
57. Kuczera, G.; Parent, E. Monte Carlo assessment of parameter uncertainty in conceptual catchment models: The Metropolis algorithm. *J. Hydrol.* **1998**, *211*, 69–85. [CrossRef]
58. Rostamian, R.; Jaleh, A.; Afyuni, M.; Mousavi, S.F.; Heidarpour, M.; Jalalian, A.; Abbaspour, K.C. Application of a SWAT model for estimating runoff and sediment in two mountainous basins in central Iran. In *Proceedings of the Hydrological Sciences Journal*; Taylor & Francis Group: Abingdon, UK, 2008; Volume 53, pp. 977–988.
59. Setegn, S.G.; Srinivasan, R.; Melesse, A.M.; Dargahi, B. SWAT model application and prediction uncertainty analysis in the Lake Tana Basin, Ethiopia. *Hydrol. Process.* **2009**, *24*, 357–367. [CrossRef]
60. Shahzad, A.; Gabriel, H.F.; Haider, S.; Mubeen, A.; Siddiqui, M.J. Development of a flood forecasting system using IFAS: A case study of scarcely gauged Jhelum and Chenab river basins. *Arab. J. Geosci.* **2018**, *11*, 383. [CrossRef]
61. CWC Central Water Commission. Available online: http://cwc.gov.in/ntbo/water-year-books (accessed on 14 May 2020).
62. Awan, S.A. Pakistan: Flood Management-River Chenab from Marala to Khanki 2003. Available online: https://www.floodmanagement.info/publications/casestudies/cs_pakistan_chenab_sum.pdf (accessed on 14 May 2020).

63. Singh, P.; Ramasastri, K.S.; Kumar, N. Topographical Influence on precipitation distribution in different ranges of Western Himalayas. *Nord. Hydrol.* **1995**, *26*, 259–284. [CrossRef]
64. Singh, P.; Jain, S.K.; Kumar, N. Estimation of Snow and Glacier-Melt contribution to the Chenab River, Western Himalaya. *Mt. Res. Dev.* **1997**, *17*, 49–56. [CrossRef]
65. Singh, D.; Gupta, R.D.; Jain, S.K. Assessment of impact of climate change on water resources in a hilly river basin. *Arab. J. Geosci.* **2015**, *8*, 10625–10646. [CrossRef]
66. Saha, S.; Moorthi, S.; Pan, H.-L.; Wu, X.; Wang, J.; Nadiga, S.; Tripp, P.; Kistler, R.; Woollen, J.; Behringer, D.; et al. The NCEP Climate Forecast System Reanalysis. *Bull. Am. Meteorol. Soc.* **2010**, *91*, 1015–1058. [CrossRef]
67. Wang, W.; Xie, P.; Yoo, S.H.; Xue, Y.; Kumar, A.; Wu, X. An assessment of the surface climate in the NCEP climate forecast system reanalysis. *Clim. Dyn.* **2011**, *37*, 1601–1620. [CrossRef]
68. Singh, S.K.; Srivastava, P.K.; Gupta, M.; Thakur, J.K.; Mukherjee, S. Appraisal of land use/land cover of mangrove forest ecosystem using support vector machine. *Environ. Earth Sci.* **2014**, *71*, 2245–2255. [CrossRef]
69. Srivastava, P.K.; Han, D.; Rico-Ramirez, M.A.; O'Neill, P.; Islam, T.; Gupta, M. Assessment of SMOS soil moisture retrieval parameters using tau-omega algorithms for soil moisture deficit estimation. *J. Hydrol.* **2014**, *519*, 574–587. [CrossRef]
70. Swain, J.B.; Patra, K.C. Streamflow estimation in ungauged catchments using regionalization techniques. *J. Hydrol.* **2017**, *554*, 420–433. [CrossRef]
71. Li, D.; Christakos, G.; Ding, X.; Wu, J. Adequacy of TRMM satellite rainfall data in driving the SWAT modeling of Tiaoxi catchment (Taihu lake basin, China). *J. Hydrol.* **2018**, *556*, 1139–1152. [CrossRef]
72. Arnold, J.G.; Moriasi, D.N.; Gassman, P.W.; Abbaspour, K.C.; White, M.J.; Srinivasan, R.; Santhi, C.; Harmel, R.D.; Griensven, A.V.; Van Liew, M.W.; et al. SWAT: Model Use, calibration, and validation. *Trans. ASABE* **2012**, *55*, 1491–1508. [CrossRef]
73. Neitsch, S.L.; Arnold, J.G.; Kiniry, J.R.; Williams, J.R. *Soil and Water Assessment Tool Theoretical Documentation Version 2009*; Texas Water Resources Institute: Temple, TX, USA, 2011.
74. Abbaspour, K.C.; Rouholahnejad, E.; Vaghefi, S.; Srinivasan, R.; Yang, H.; Kløve, B. A continental-scale hydrology and water quality model for Europe: Calibration and uncertainty of a high-resolution large-scale SWAT model. *J. Hydrol.* **2015**, *524*, 733–752. [CrossRef]
75. Nash, J.E.; Sutcliffe, J.V. River flow forecasting through conceptual models part I - A discussion of principles. *J. Hydrol.* **1970**, *10*, 282–290. [CrossRef]
76. Moriasi, D.N.; Arnold, J.G.; Van Liew, M.W.; Bingner, R.L.; Harmel, R.D.; Veith, T.L. Model Evaluation Guidelines for Systematic Quantification of Accuracy in Watershed Simulations. *Trans. ASABE* **2007**, *50*, 885–900. [CrossRef]
77. Santhi, C.; Arnold, J.G.; Williams, J.R.; Dugas, W.A.; Srinivasan, R.; Hauck, L.M. Validation of The swat model on a Large Rwer Basin with point and nonpoint sources. *J. Am. Water Resour. Assoc.* **2001**, *37*, 1169–1188. [CrossRef]
78. Gupta, H.V.; Sorooshian, S.; Yapo, P.O. Status of Automatic Calibration for Hydrologic Models: Comparison with Multilevel Expert Calibration. *J. Hydrol. Eng.* **1999**, *4*, 135–143. [CrossRef]
79. Van Liew, M.W.; Arnold, J.G.; Bosch, D.D. Problems and Potential of Autocalibrating a Hydrologic Model. *Trans. ASAE* **2005**, *48*, 1025–1040. [CrossRef]
80. Eckhardt, K.; Fohrer, N.; Frede, H.-G. Automatic model calibration. *Hydrol. Process.* **2005**, *19*, 651–658. [CrossRef]
81. Willmott, C.J.; Robeson, S.M.; Matsuura, K. A refined index of model performance. *Int. J. Climatol.* **2012**, *32*, 2088–2094. [CrossRef]
82. Taylor, K.E. Summarizing multiple aspects of model performance in a single diagram. *J. Geophys. Res. Atmos.* **2001**, *106*, 7183–7192. [CrossRef]